

## Interfacial dynamics in demixing systems with ultralow interfacial tension

D G A L Aarts<sup>1</sup>, R P A Dullens and H N W Lekkerkerker

Van't Hoff Laboratory, Debye Research Institute, University of Utrecht,  
Padualaan 8, 3584 CH Utrecht, The Netherlands

E-mail: [d.g.a.l.aarts@chem.uu.nl](mailto:d.g.a.l.aarts@chem.uu.nl)

*New Journal of Physics* **7** (2005) 40

Received 7 October 2004

Published 4 February 2005

Online at <http://www.njp.org/>

doi:10.1088/1367-2630/7/1/040

**Abstract.** We report measurements on fluid–fluid phase separation in a colloid–polymer mixture, which can be followed in great detail due to the ultralow interfacial tension. The use of the real-space technique, laser-scanning confocal microscopy, leads to clear, well-defined images making quantitative comparisons to theory possible and being highly instructive. Simple scaling arguments are given why, in experiment, three steps of the phase separation can be observed: an interfacial-tension-driven coarsening, gravity-driven flow and finally the interface formation. All these processes are observed in a single experiment. The first stage can be quantitatively described by viscous hydrodynamics. Coarsening occurs through pinch-off events. The second stage begins at a typical size of  $\sim 2\pi$  times the capillary length reminiscent of the Rayleigh–Taylor instability. The liquid phase breaks up and becomes discontinuous. There is strong directional flow in the system, but the Reynold's number remains much smaller than unity. Finally, the macroscopic interface is formed, growing upwards, with a velocity comparable to the coarsening velocity in the initial stage. Again, viscous hydrodynamics apply with a characteristic velocity of the interfacial tension over the viscosity.

<sup>1</sup> Author to whom any correspondence should be addressed.

## Contents

1. Introduction	2
2. Length- and timescales	3
3. Experimental system and method	5
4. Initial phase separation	6
5. Gravity-driven flow	8
6. Macroscopic interface formation	10
7. Conclusion	11
Acknowledgments	11
References	12

## 1. Introduction

The study of the morphology and kinetics of phase separation processes follows a long tradition and remains of fundamental importance [1]. The early initial stages of the phase separation are determined by the underlying free-energy landscape, whereas the observed morphology kinetically depends on characteristic fluid properties as well [2], of which the viscosity and interfacial tension are the most important ones. Here, we present a real-space study of the effects of an ultralow interfacial tension on the phase separation kinetics in a fluid–fluid demixing colloid–polymer mixture. This is not only of fundamental importance, but has industrial relevance as well. For example, in the food industry, extensive use is made of the properties of polymers, e.g. to invoke gelation [3], and adding these to food suspensions leads effectively to colloid–polymer mixtures [4].

Phase separating colloid–polymer mixtures are well known to display a behaviour similar to molecular fluid–fluid demixing systems [5]. The coexisting phases are a colloidal liquid (rich in colloid and poor in polymer) and a colloidal gas (poor in colloid and rich in polymer). The origin of the phase separation lies in the entropy-driven attraction between the colloids, which is mediated by the polymers [6, 7]. It is known from experiment [8]–[11] and theory [12]–[14] that in such systems the interfacial tension  $\gamma$  scales as  $\gamma \sim k_B T/d^2$ , with  $k_B T$  the thermal energy and  $d$  particle diameter, leading to ultralow values for the interfacial tension.

We use laser-scanning confocal microscopy (LSCM) to follow the processes of phase separation. This real-space technique leads to clear, well-defined images of the several stages of phase separation. Hence, the purpose of this paper is to study the effects of the ultralow interfacial tension and present images and movies which we believe to be instructive and might assist in a further development of theories on demixing.

Experimentally, the phase-separation process can roughly be divided into three stages, which will be made apparent by a consideration of the relevant length- and timescales in demixing systems (section 2). Once the sharp interfaces have been formed, the interfacial tension drives the coarsening of the spinodal structure (section 4), which is followed by a gravity-driven collapse and flow of the spinodal network (section 5) and finally, a sharp macroscopic interface is formed and the phase separation is completed (section 6). These sections will be preceded by a brief description of the experimental system and methods (section 3) and our findings will be summarized in section 7.

## 2. Length- and timescales

In the unstable region of the phase diagram each density fluctuation in an initially homogeneous system is energetically favourable, but fluctuations with large wavelengths and hence shallow-density gradients are thermodynamically more favourable, whereas for short wavelengths particles only have to diffuse over short distances. This competition leads to a fastest growing mode  $q_m$  within the framework of Cahn–Hilliard theory of [15]–[18]

$$q_m^2 = -\frac{1}{2\kappa} \left( \frac{\partial\mu}{\partial n} \right), \quad (1)$$

where  $\kappa$  is the Cahn–Hilliard square-gradient coefficient [15, 16] (like the van der Waals square-gradient coefficient),  $n$  the overall number density and  $\mu$  the chemical potential. The wavelength  $L \equiv 2\pi/q_m$  that follows from (1) is a few times the particle diameter  $d$  for colloid–polymer mixtures away from the critical point, of similar magnitude as for example estimated by van Aartsen for demixing polymer–polymer mixtures [19] and which we here estimated by using the theory presented in [20]. As time proceeds the system approaches its equilibrium densities and the gradients in the density get steeper [21].

At the same time the system coarsens and  $L$  grows in the diffusive regime as [22]

$$L(t) = \left( \frac{k_B T}{\eta} t \right)^{1/3}. \quad (2)$$

A simple way to understand this diffusive coarsening is by considering the velocity of an object of size  $L$  driven by chemical potential gradients of magnitude  $\propto k_B T/L$ , i.e.

$$\frac{dL}{dt} = \frac{-\nabla\mu}{f} \propto \frac{k_B T/L}{\eta L}, \quad (3)$$

with  $k_B T$  the thermal energy,  $f$  the friction of magnitude  $\eta L$  and  $\eta$  the viscosity. Integrating (3) immediately leads to (2).

Upon the formation of sharp interfaces, the interfacial tension  $\gamma$  starts playing a role. Here, we will follow didactic derivations of especially Siggia [22] and Bray [23]. A more extended scaling analysis is given by Kendon *et al* [24]. The dynamics are governed by the Navier–Stokes equations

$$\rho D_t \mathbf{u} = \eta \nabla^2 \mathbf{u} - \nabla p - g \Delta \rho \mathbf{e}_3. \quad (4)$$

The left-hand side of (4), with  $\rho$  the mass density,  $D_t$  the material derivative and  $\mathbf{u}$  the velocity, captures the inertial terms and is much smaller than the viscous dissipation—the first term of the right-hand side of (4)—if the Reynold’s number is small. The last term accounts for the hydrostatic pressure where  $g$  is earth’s constant of acceleration,  $\Delta \rho$  the mass density difference between the two phases and  $\mathbf{e}_3$  a unit vector pointing along gravity. For small  $L$ , gravity is not yet important and the interplay between viscous dissipation and gradients in the pressure  $p$  due to the Laplace pressure,

$$\eta \nabla^2 \mathbf{u} \propto \eta \frac{1}{L^2} u \quad \text{and} \quad \nabla p \propto \frac{1}{L} \frac{\gamma}{L}, \quad (5)$$

leads to a (capillary) velocity in the viscous hydrodynamic regime of

$$u \propto \frac{\gamma}{\eta} \quad (6)$$

of which the prefactor was estimated to be  $\sim 0.1$  [22]. In extensive computer simulations of two incompressible fluids of maximal symmetry, i.e. identical viscosity, density and volume fraction of the two fluids, this prefactor has been determined for the first time and was found to be 0.072 [24, 25]. The magnitude of this interface velocity becomes comparable to the diffusive coarsening velocity of (3) at a cross-over length of [22]

$$L \propto \sqrt{\frac{k_B T}{\gamma}}. \quad (7)$$

From there on the system coarsens linearly with time proportional to (6).

At a Reynold's number  $Re = \rho u L / \eta$  of order one, inertial terms start playing a role. Using the capillary velocity (6) as the characteristic velocity we find that at a cross-over length of

$$L \propto \frac{\eta^2}{\rho \gamma}, \quad (8)$$

the inertial hydrodynamic regime is entered (see for example [23]). The balance between gradients in pressure (see (5)) and inertia

$$\rho D_t \mathbf{u} \propto \rho \frac{L}{t^2} \quad (9)$$

then leads to a coarsening of [23]

$$L(t) \propto \left( \frac{\gamma}{\rho} t^2 \right)^{1/3}. \quad (10)$$

This  $t^{2/3}$ -regime was first predicted by Furukawa [26]. Finally, the gravity term in (4) becomes as large as the Laplace pressure (5) at [22],

$$L \propto \sqrt{\frac{\gamma}{g \Delta \rho}} \equiv l_{\text{cap}}, \quad (11)$$

which is precisely the capillary length  $l_{\text{cap}}$  and the phase separation becomes gravity-driven.

During this gravity-driven flow, we find in our experiment that one of the phases becomes discontinuous—in our case the heavy liquid phase—and the interface emerges at the bottom of the container. Individual droplets sediment towards the emerging interface. They form a structure of droplets on top of each other which resembles a foam. For ultralow interfacial tensions, the coalescence is governed by viscous forces and inertial terms do not play a role. Again, the capillary velocity (6) sets the velocity scale and after all droplets of both phases have coalesced, the system is fully phase-separated.

In molecular systems, where the interfacial tension is relatively large, inertial terms may be expected to become important at lengths smaller than the capillary length (for estimates of

the lengths in both molecular and colloid–polymer mixtures, see for example [10]). However, in experiments with molecular fluids, the inertial regime has not yet been observed [1]. Of course, the prefactor of (6), i.e. 0.072, can be used in the estimate of (8), and this postpones the inertial regime to larger lengthscales, although this factor alone does not suffice as explanation. In the aforementioned simulations [24, 25, 27], in which the inertial regime is observed, it is clearly found that inertial terms do not become dominant immediately at  $Re = 1$ . The cross-over from the viscous to the inertial hydrodynamic regime is very broad and inertia becomes dominant at much larger Reynold’s numbers. In that case the length scales are much larger as well, of the order of the capillary length, and gravity comes into play, which provides a further explanation of the lack of experimental evidence for the occurrence of the inertial regime. In clear contrast to molecular systems, colloidal systems are expected to remain for long periods of time in the viscous regime and—following the above scaling arguments—gravity-driven flow occurs well before the inertial regime. Furthermore, during the interface formation inertial terms do not play a role in the case of colloid–polymer mixtures.

### 3. Experimental system and method

We prepared fluorescent poly(methylmethacrylate) (PMMA) colloidal spheres following the method of Bosma *et al* [28] slightly modified by using *cis/trans*-decalin (Merck, for synthesis) as the reaction solvent. The (dynamic light scattering) radius  $R_c$  was 25 nm and the polydispersity was less than 10%, estimated from scanning electron microscopy images. A commercially available polymer polystyrene (Fluka) was used with a molecular weight  $M_w = 233 \text{ kg mol}^{-1}$  ( $M_w/M_n = 1.06$ , with  $M_n$  the number average molecular weight) and a radius of gyration  $R_g$  of  $\sim 14 \text{ nm}$  (calculated from data in the literature [29]). Both species were dispersed in decalin and since all densities were known, mass fractions could be directly converted to volume fractions of colloids,  $\phi_c = \frac{4}{3}\pi R_c^3 n_c$ , and of polymers,  $\phi_p = \frac{4}{3}\pi R_g^3 n_p$ , where  $n_c$  and  $n_p$  are the number densities of colloids and polymers, respectively. Samples were prepared by mixing colloid- and polymer-stock dispersions and diluting with decalin. At high polymer concentrations, it took a few hours before the system phase-separated completely, at intermediate concentrations about 15 min and very close to the binodal again up to hours. The resulting macroscopic interface was always very sharp. In principle, the size ratio  $q = R_g/R_c = 0.56$  allows for the observation of gas, liquid and crystal phases [30], but only gas–liquid phase coexistence was observed. The complete phase diagram has been published elsewhere [31]. Fluid–crystal coexistence was possibly suppressed by the polydispersity of the spheres as is often the case in systems with small spheres and the system gelled instead of displaying a crystal phase at relatively high polymer concentrations.

To study the colloid–polymer mixtures, we used a laser scanning confocal head (Nikon C1) mounted on a horizontally placed light microscope (Nikon Eclipse E400). Large glass cuvettes (of volume  $\sim 1 \text{ cm}^3$ ) with extra thin cover glass walls (0.17 mm thick) were fabricated in our laboratory. The microscope detects the fluorescence of excited dye in the colloids, while the solvent and polymers remain dark. Hence the colloidal-rich phase (liquid) appears bright, whereas the colloidal-poor phase (gas) appears dark. We used low numerical aperture objectives in order to have a larger field of view and to obtain some three-dimensional information instead of imaging only a very thin slice.

In the present paper, we focus on a sample with  $\phi_c = 0.076$  and  $\phi_p = 0.50$ , which is reasonably close to the critical point. The complete phase separation took about 20 min, of which

the initial coarsening took 50 s (section 4), the gravity-driven flow in the middle of the sample 5 min (section 5) and the interface formation the remaining time (section 6). Other statepoints show basically similar behaviour, except if close to the binodal the metastable region is entered where phase separation proceeds via nucleation and growth. We obtained an interfacial tension of  $\gamma = 2 \times 10^{-7} \text{ N m}^{-1}$  by analysing the thermally induced capillary waves in a similar manner as done in [11] and a capillary length of  $l_{\text{cap}} = 17.6 \mu\text{m}$  by measuring the colloidal gas–colloidal liquid interfacial profile close to a wall [10]. The densities of the gas and liquid phases have been measured with an Anton Paar density metre resulting in a density difference of  $\Delta\rho = 53 \text{ kg m}^{-3}$  and via (11) to  $\gamma = 1.6 \times 10^{-7} \text{ N m}^{-1}$ , in good agreement with the capillary wave approach. Furthermore, the viscosities of the two phases have been measured on an Anton Paar Physica MCR300 rheometer giving  $\eta_G = 8 \text{ mPa s}$  for the gas (G) phase and  $\eta_L = 31 \text{ mPa s}$  for the liquid (L) phase (slightly larger than the value reported in [31]). Finally, the diffusion coefficients in the gas and liquid phases have been measured by performing real-space fluorescence recovery after photobleaching experiments as explained in more detail in [31, 32]. The diffusion coefficient in the liquid phase was  $D = 4.9 \times 10^{-13} \text{ m}^2 \text{ s}^{-1}$  and in the gas phase  $D = 1.9 \times 10^{-12} \text{ m}^2 \text{ s}^{-1}$ , measured after the phase separation is completed.

During the homogenization of the colloid–polymer mixture, air bubbles can be present in the system. When they escape, the spinodal structure is destroyed and this immediately leads to individual drops. Besides that, in the top of the sample drops are formed much earlier. Therefore, we carefully homogenized the sample to minimize the number of air bubbles and always imaged at the final interface position.

#### 4. Initial phase separation

Directly after homogenization, the phase separation starts. From the bicontinuous structure in figure 1 it is immediately clear that the system separates through spinodal decomposition. Already in the first images, which are taken 3 s after homogenization, the interfaces are sharp and the system coarsens linearly with time as will be shown below. This is similar to the observations made in [33], where the focus of the work lay on the initial stage of phase separation. From the estimates of (1) and (7), we find that the linear-response region of Cahn–Hilliard theory takes a very short time, as does the diffusive regime with the  $t^{1/3}$  coarsening. Colloids only have to diffuse over a few times their own diameter before the viscous hydrodynamic regime is reached. From the colloidal diffusion coefficients in the gas and liquid phases (section 3), we see that the viscous regime is reached in less than a second and therefore the preceding regimes are not observed.

The system can coarsen via coalescence or pinch-off events. In two-dimensions such events are similar, but in three-dimensions they are distinctly different and here the system mostly coarsens through pinch-off. In the bottom row of figure 1 such an event is marked and the insets in figure 1(e) show a zoom-in of this event. During a pinch-off, the liquid bridge drains and snaps more or less symmetrically at a certain point. According to simulations by Cates and co-workers [27], the retracting tips might evaporate a bit, but we do not have sufficient space and time resolution to determine this. There is no recoil and an overdamped relaxation. By carefully inspecting movie 1 many more similar events can be observed, especially of snapping liquid necks surrounded by gas phase, since the liquid has a stronger fluorescence than the gas phase.

The collective overdamped motion of the interface leads to a coarsening of the spinodal structure. One possible way to analyse the structure was clearly demonstrated by



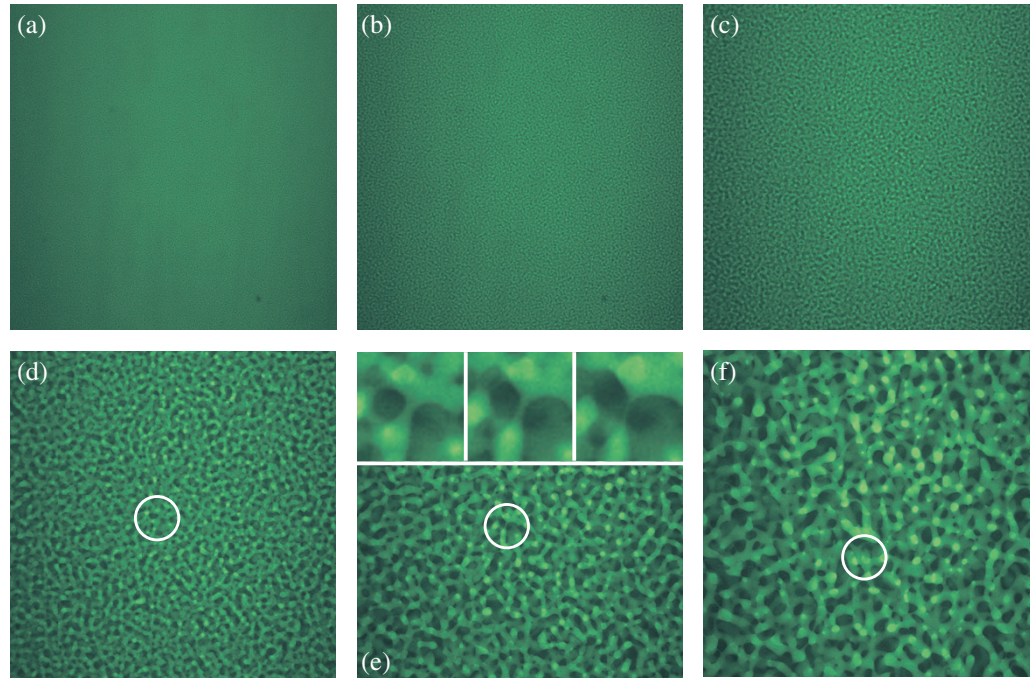


**Figure 1.** LSCM images ( $1400 \times 1400 \mu\text{m}^2$ ) of a phase separating colloid–polymer mixture. Gravity points downwards (in all images). Directly after homogenization a spinodal structure is observed ((a)  $t = 3$  s), which immediately coarsens in time ((b)  $t = 7$  s) and ((c)  $t = 11$  s). From ((d)  $t = 22$  s), it is evident that coarsening occurs through pinch-off instead of coalescence and one can follow such events in time ((e)  $t = 33$  s) and ((f)  $t = 45$  s). The white circle marks such an event, which becomes more apparent by carefully studying [movie 1](#). The insets ( $109 \times 109 \mu\text{m}^2$ ) zoom in on the pinch-off event (from left to right,  $t = 29, 33, 37$  s).

Hashimoto *et al* [34], who, in a first-time study, performed LSCM experiments on spinodally demixing polymer mixtures and paid special attention to the topology of the spinodal structure. Here, we are interested in the coarsening rate, which can best be quantified by performing discrete Fourier transforms of the LSCM images, see for example the inset of figure 2(a), which shows the Fourier transform of figure 1(c). The Fourier transforms are radially averaged (see figure 2(a)). In [31] we showed that the structure factors obtained in such a manner scaled dynamically and that the shape of the curves followed predictions by Furukawa [35], which is also the case for the present state-point, but it is not the topic of the article.

The position of the maximum intensity shifts inwards as a function of time. The position  $k_{\text{max}}$  corresponds to a length  $L = L_{\text{image}}/k_{\text{max}}$ , where  $L_{\text{image}}$  is the image width. In figure 2(b),  $L$  is plotted as a function of time. There is an initial linear increase in time;  $L$  coarsens with a velocity of  $1.94 \mu\text{m s}^{-1}$  over the first 30 s. For longer times determining the typical size  $L$  by Fourier transforming becomes more unreliable. From (6) and the quantities for the interfacial tension and the viscosities (section 3) a velocity of  $\gamma/\eta_L \sim 6 \mu\text{m s}^{-1}$  up to  $\gamma/\eta_G \sim 25 \mu\text{m s}^{-1}$  is obtained, which is directly connected to the measured coarsening velocity, but in a complicated manner. As mentioned in section 2 direct simulations [24, 25] point to a prefactor of 0.072 in (6),

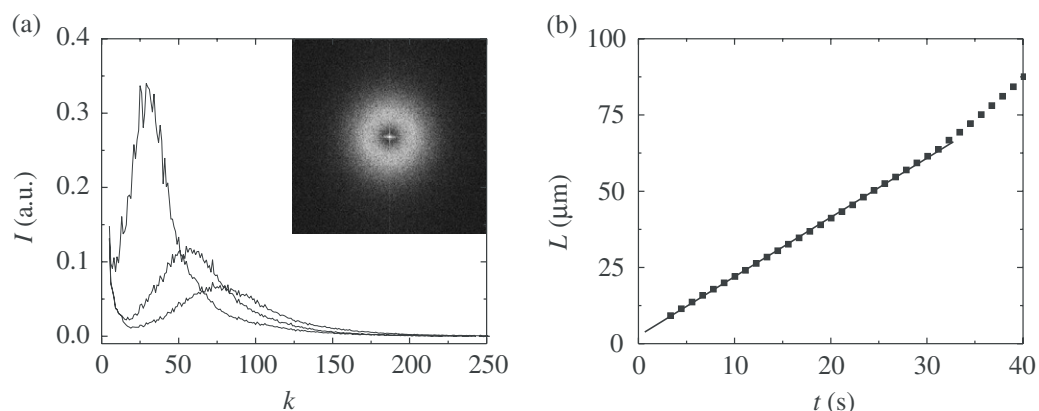


**Figure 2.** (a) Radial averages of the Fourier transforms for times 7, 11 and 22 s showing a shift in the position of the maximum intensity to smaller  $k$  values. One pixel in  $k$ -space corresponds to  $2\pi$  over the image width  $L_{\text{image}}$ . The intensity increase at small  $k$  values stems from instrument properties and contains no relevant physical information. From the positions of the maximum intensity the characteristic length  $L$  can be obtained, which is plotted as a function of time in (b), where the full line is a linear fit up to the first 30 s. The inset in (a) shows the discrete Fourier transform of the LSCM image in figure 1(c).

but the simulations were performed for a symmetric fluid–fluid mixture of equal viscosity, which is not the experimental situation. Considering the spinodal structure as constructed from many individual fluid (both gas and liquid) cylinders can shed some light on the different terms at play. The breakup rate of a viscous cylinder surrounded by another viscous fluid depends on both the viscosities, the initial distortions and the radius of the cylinder [36]. Taking only the inner viscosity into account gives a reasonable estimate of the breakup rate [37] and leads to  $\gamma/\eta_L$  for liquid and  $\gamma/\eta_G$  for gas cylinders. For cylinders, the prefactor of (6) can become of the order of 0.01 or smaller [37], but the prefactor might be much larger given the already heavily curved (i.e. distorted) interconnected structure in the spinodal case. Finally, since there is eventually approximately 70% gas and 30% liquid phase, the gas phase must consist of thicker ‘cylinders’, which break up slowly. Since both phases initially stay continuous, both breakup rates, and hence both velocities ( $\gamma/\eta_L$  and  $\gamma/\eta_G$ ) might play a role. The measured velocity is thus a non-trivial combination of the aforementioned terms, eventually leading to  $1.94 \mu\text{m s}^{-1}$ .

## 5. Gravity-driven flow

The spinodal structure starts to collapse under its own weight after about 36 s at  $L = 75 \mu\text{m}$ . There is still some coarsening. From about 49 s, i.e.  $L \sim 100 \mu\text{m}$ , the scattering rings flatten off and there is a clear gravity-driven flow (see figure 3(a)). The cross-over from the viscous regime to the gravity-driven regime is not sharp, but takes about 15 s. Since relatively heavy and light materials are mixed together, the gravity-driven flow is reminiscent of the Rayleigh–Taylor instability [38, 39]. In our case, the fastest growing mode of the Rayleigh–Taylor instability is larger than the capillary length, but modes with wavelengths of  $2\pi l_{\text{cap}}$  are already unstable, in good agreement with the observations and the scaling estimate (11).



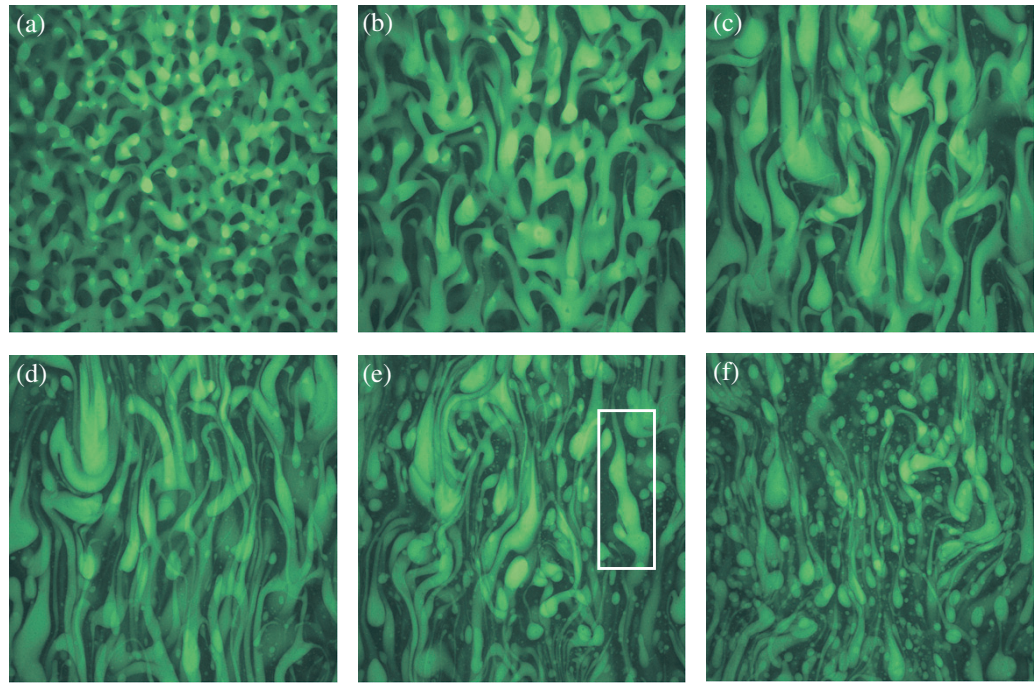


**Figure 3.** LSCM images ( $1400 \times 1400 \mu\text{m}^2$ ) of gravity-driven flow in a phase separating colloid–polymer mixture. In ((a)  $t = 56$  s) the spinodal structure is collapsing under its own weight leading to strong flow in ((b), (c) and (d):  $t = 72$ , 89 and 106 s, respectively). Not much coarsening occurs. (d) The onset to a transition with vertical lanes is observed. ((e)  $t = 134$  s) and ((f)  $t = 178$  s) individual droplets become more apparent. The white box in (e) marks a Rayleigh instability. See also [movie 2](#).

From then on there is a strong flow as well as backflow in the system (see figures 3(b) and (c)). Sedimenting objects drag other objects along with them leading to directional flow (lane-like structures) and larger sedimenting objects. The largest droplet-shaped objects have a maximum thickness of  $\sim 200 \mu\text{m}$  and sediment with a velocity of up to about  $70 \mu\text{m s}^{-1}$ . The Reynolds number, however, remains much smaller than one ( $\sim 10^{-3}$ ). There is not much coarsening in the width of the lanes as can be seen by comparing the structures in figures 3(c) and (d). The vertical lanes have a width of about  $100 \mu\text{m}$  decreasing to  $30 \mu\text{m}$  at later times. For the present statepoint, the liquid phase is the minority phase occupying approximately 30% of the volume. It breaks up, whereas the gas phase remains continuous. During the flow, a transition to regular lanes of heavy phase going down and light phase going up can occur as seen in a mixture of Teflon spheres and xanthan polymer [40, 41] and in a mixture of silica colloids and poly(dimethylsiloxane) in cyclohexane [10]. Recently, Wysocki and Löwen theoretically studied similar phenomena in driven colloidal mixtures and found for not too large driving forces good agreement with the classical Rayleigh–Taylor instability [42]. Such a formation of lanes is clearly a very efficient way to separate the phases. In experiments under shear such lanes are often observed, see for example [1, 43, 44], and in the present system the onset of the transition is observed, see figure 3(d), but does not reach the point of distinct lanes. Apparently, either gravity is not strong enough to drive this transition or it takes too long, such that most of the material has already separated.

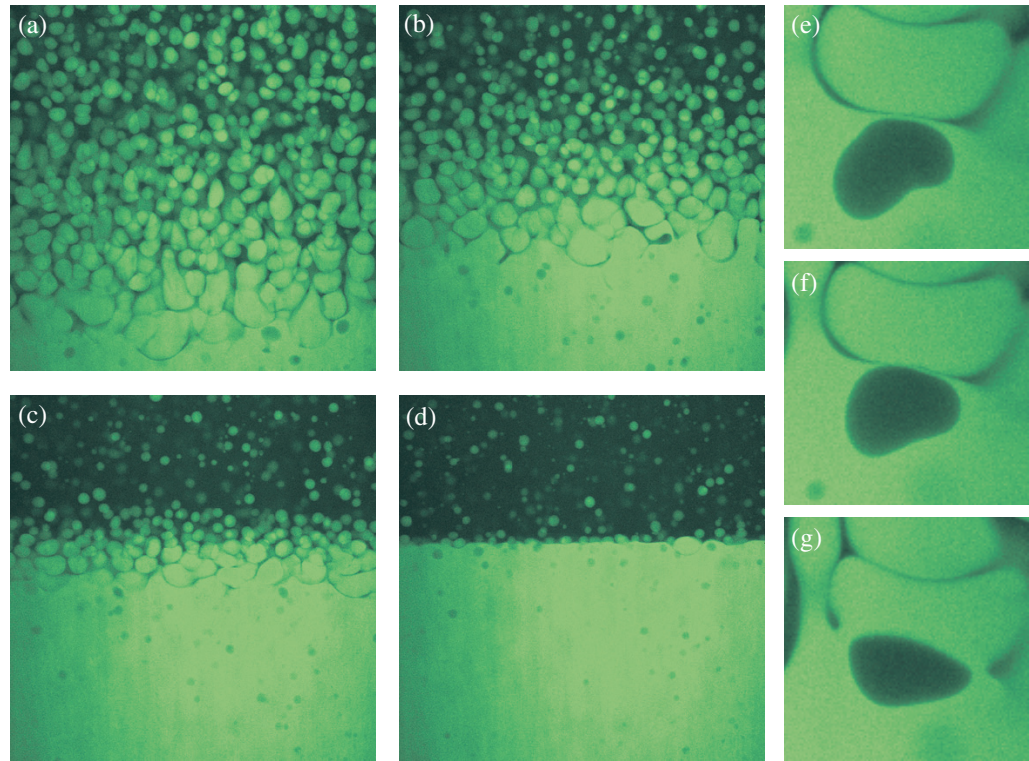


**Figure 4.** LSCM images ( $1400 \times 1400 \mu\text{m}^2$ ) of interface formation in a colloid–polymer mixture taken after 9, 13, 16 and 20 min after homogenization (a)–(d). In (e)–(g) an example ( $171 \times 171 \mu\text{m}^2$ ) is shown of a coalescence event induced by the gas bubble with (f) 5 s and (g) 15 s after (e). See also [movie 3](#) of images (a)–(d).

During the flow not many individual drops are formed. Only at the final stages of the flow more and more droplets can be observed (see figures 3(e) and (f)). The liquid cylinders are then thin enough that a Rayleigh instability [38] can grow and cause breakup, indicated by the white box in figure 3(e). Furthermore, the sedimenting objects disturb each other and this causes additional breakups.

## 6. Macroscopic interface formation

In the present example, the interface grows from the bottom. The elongated drops become more spherical again close to the forming interface, while the gravity-driven structure is still present well above the interface. At the end of the gravity-driven flow, drops coalesce with their bulk phase (see figure 4). Gas droplets inside the liquid phase follow the same pattern. The coalescence is a three-step process; the continuous phase drains, a first connection is made and the material is pushed into the bulk phase. The first step is time consuming: the rate of thinning of the continuous phase is proportional to the viscosity of the continuous phase and to the fourth power of the exposed length of the droplet [45]. In the second step, the dynamic roughness of fluid interfaces plays an important role and facilitates the formation of a connection [11]. Moreover, rising gas bubbles induce the breakup as can be seen in figures 4(e)–(g). In the third step, the

dynamics are initially governed by viscous hydrodynamics leading to a linear time dependence of the coalescence [46]. Since the interfacial tension is so small, this remains the case and inertia does not become important. In case of molecular fluids it does [47].

In the last stages of the interface formation, the interface rises with a velocity of approximately  $1.5 \mu\text{m s}^{-1}$ , very similar to the coarsening velocity in the viscous hydrodynamic regime, i.e. proportional to (6). Structurally, it is similar to the collapse of an inverse foam. Finally, a sharp interface is formed (see figure 4(d)). Some individual drops still have to coalesce, especially small droplets. Their sedimentation velocity ( $6.4 \mu\text{m s}^{-1}$  for a droplet of radius  $20.5 \mu\text{m}$ ) is in good agreement with the modified Stokes equation for sedimenting spheres with a finite viscosity [38].

## 7. Conclusion

Simple scaling arguments have been given for the consecutive stages of fluid–fluid phase separation in a colloid–polymer mixture. In principle, a different route is expected to be followed compared with that in molecular systems, where the inertial regime is entered before gravity-driven flow, although in experiments with molecular fluids, the inertial regime has not yet been observed. The scaling arguments make evident that in experiments three successive steps can be observed. In the first step, the spinodal pattern coarsened by means of pinch-off events. The preceding linear Cahn–Hilliard regime and the diffusive regime were experimentally not observed. Colloids only have to diffuse over a few times their own particle diameter to reach the viscous regime and this is rapidly so, as can be understood from the diffusion coefficients. In fact, only in a few systems the linear Cahn–Hilliard regime has been observed, e.g. in polymer–polymer systems [48]–[50], and the cross-over between the diffusive and the viscous regime has been observed for example in [51, 52] for binary fluid mixtures.

By Fourier transforming the LSCM images the characteristic size  $L$  was seen to increase linearly with time proportional to  $\gamma/\eta$  (6), the characteristic velocity in the viscous hydrodynamic regime, although the prefactor and the precise definition of  $\eta$  in (6) are difficult to estimate given the large number of terms at play and the complexity of the spinodal structure. At a typical size  $L \sim 2\pi l_{\text{cap}}$ , the structural collapsed due to gravity, which is reminiscent of the Rayleigh–Taylor instability. There was still some coarsening. The minority phase, the liquid, broke up and became discontinuous for reasons possibly related to the breakup rates of fluid cylinders. Due to the flow, the liquid and gaseous material quickly separated and the interface grew upwards via droplet coalescence. The growth rate was similar to the coarsening rate in the initial stage and the system remained in the viscous hydrodynamic regime. Finally, the use of LSCM leads to clear and well-defined images and movies, which are instructive and might inspire further theoretical development.

## Acknowledgments

We thank Hanneke van der Wiel and Susan Kersjes for pioneering experiments and Jan Dhont for useful discussions. This work was supported by the Stichting voor Fundamenteel Onderzoek der Materie (Foundation for Fundamental Research on Matter), which is part of the Nederlandse Organisatie voor Wetenschappelijk Onderzoek (Netherlands Organisation for Advancement of Research).



## References

- [1] Onuki A 2002 *Phase Transition Dynamics* (Cambridge: Cambridge University Press)
- [2] Binder K 1990 Spinodal decomposition *Phase Transformations in Materials* vol 5 (Weinheim: VCH) pp 405–71
- [3] Lorén N, Alstkr A and Hermansson A M 2001 *Macromolecules* **34** 8117
- [4] Dickinson E and Walstra P 1993 *Food Colloids and Polymers: Stability and Mechanical Properties* (Cambridge: Royal Society of Chemistry)
- [5] Verhaegh N A M and Lekkerkerker H N W 1997 *Proc. Int. School of Physics 'Enrico Fermi'* ed F Mallamace and H E Stanley (Amsterdam) pp 347–81
- [6] Asakura S and Oosawa F 1954 *J. Chem. Phys.* **22** 1255–6
- [7] Vrij A 1976 *Pure Appl. Chem.* **48** 471–83
- [8] de Hoog E H A and Lekkerkerker H N W 1999 *J. Phys. Chem. B* **103** 5274–9
- [9] de Hoog E H A and Lekkerkerker H N W 2001 *J. Phys. Chem. B* **105** 11636–40
- [10] Aarts D G A L, van der Wiel J H and Lekkerkerker H N W 2003 *J. Phys.: Condens. Matter* **15** S245–S250
- [11] Aarts D G A L, Schmidt M and Lekkerkerker H N W 2004 *Science* **304** 847
- [12] Vrij A 1997 *Physica A* **235** 120–8
- [13] Brader J M and Evans R 2000 *Europhys. Lett.* **49** 678–84
- [14] Brader J M, Evans R, Schmidt M and Löwen H 2002 *J. Phys.: Condens. Matter* **14** L1–L8
- [15] Cahn J W and Hilliard J E 1958 *J. Chem. Phys.* **28** 258
- [16] Cahn J W and Hilliard J E 1959 *J. Chem. Phys.* **31** 688
- [17] Cahn J W 1961 *Acta Metall.* **9** 795
- [18] Cahn J W 1965 *J. Chem. Phys.* **42** 93
- [19] van Aartsen J J 1970 *Eur. Polym. J.* **6** 919
- [20] Aarts D G A L, Dullens R P A, Lekkerkerker H N W, Bonn D and van Roij R 2004 *J. Chem. Phys.* **120** 1973
- [21] Dhont J K G 1996 *An Introduction to Dynamics of Colloids* (Amsterdam: Elsevier)
- [22] Siggia E D 1979 *Phys. Rev. A* **20** 595–605
- [23] Bray A J 2000 Coarsening dynamics of nonequilibrium phase transitions *Soft and Fragile Matter: Nonequilibrium Dynamics, Metastability and Flow* ed M E Cates and M R Evans (Edinburgh: SUSSP Publications, Institute of Physics Publishing)
- [24] Kendon V M, Cates M E, Pagonabarraga I, Desplat J-C and Bladon P 2001 *J Fluid Mech.* **440** 147
- [25] Kendon V M, Desplat J-C, Bladon P and Cates M E 1999 *Phys. Rev. Lett.* **83** 576
- [26] Furukawa H 1985 *Phys. Rev. A* **31** 1103
- [27] Pagonabarraga I, Desplat J-C, Wagner A J and Cates M E 2001 *New J. Phys.* **3** 9.1
- [28] Bosma G, Pathmamanoharan C, de Hoog E H A, Kegel W K, van Blaaderen A and Lekkerkerker H N W 2002 *J. Colloid Interface Sci.* **245** 292–300
- [29] Berry G C 1966 *J. Chem. Phys.* **44** 4550
- [30] Lekkerkerker H N W, Poon W C K, Pusey P N, Stroobants A and Warren P B 1992 *Europhys. Lett.* **20** 559–64
- [31] Aarts D G A L and Lekkerkerker H N W 2004 *J. Phys.: Condens. Matter* **16** S4231
- [32] Simeonova N and Kegel W K 2003 *Faraday Discuss.* **123** 27
- [33] Verhaegh N A M, van Duijneveldt J S, Dhont J K G and Lekkerkerker H N W 1996 *Physica A* **230** 409–36
- [34] Hashimoto T, Koga T, Jinnai H and Nishikawa Y 1998 *Nuovo Cimento* **20** 1947
- [35] Furukawa H 1984 *Physica A* **123** 497
- [36] Tomotika S 1935 *Proc. R. Soc. A* **150** 322
- [37] Lekkerkerker H N W and de Hoog E H A 2001 *Physica A* **298** 69
- [38] Lamb H 1932 *Hydrodynamics* (Cambridge: Cambridge University Press)
- [39] Chandrasekhar S 1981 *Hydrodynamic and Hydromagnetic Stability* (New York: Dover)
- [40] Aarts D G A L 2003 *Faraday Discuss.* **123** 174
- [41] Koenderink G H, Aarts D G A L, de Villeneuve V W A, Philipse A P, Tuinier R and Lekkerkerker H N W 2003 *Biomacromolecules* **4** 129

- [42] Wysocki A and Löwen H 2004 *J. Phys.: Condens. Matter* **16** 7209
- [43] Hashimoto T, Matsuzaka K, Moses E and Onuki A 1995 *Phys. Rev. Lett.* **74** 126–9
- [44] Matsuzaka K, Koga T and Hashimoto T 1998 *Phys. Rev. Lett.* **80** 5441–4
- [45] Brown A H and Hanson C 1967 *Nature* **214** 76–7
- [46] Eggers J, Lister J R and Stone H A 1999 *J. Fluid Mech.* **401** 293–310
- [47] Duchemin L, Eggers J and Josserand C 2003 *J. Fluid Mech.* **487** 167
- [48] Izumitani T and Hashimoto T 1985 *J. Chem. Phys.* **83** 3694
- [49] Okada M and Han C C 1986 *J. Chem. Phys.* **85** 5317
- [50] Bates F S and Wiltzius P 1989 *J. Chem. Phys.* **91** 3258
- [51] Kim M W, Schwartz A J and Goldburg W L 1978 *Phys. Rev. Lett.* **41** 657
- [52] Chou Y C and Goldburg W I 1979 *Phys. Rev. A* **20** 2105